REFERENCES

[1] M. S. Gupta and R. J. Lomax, "A current-excited large-signal analysis of IMPATT diodes and its circuit implications," *IEEE Trans. Electron Devices,* vol. ED-20, pp. 395–399, April 1973.

[2] M. S. Gupta and R. J. Lomax, "A self-consistent large-signal analysis of a Read-type IMPATT diode oscillator," *IEEE Trans. Electron Devices,* vol. ED-18, pp. 544–550, Aug. 1971.

[3] W. J. Evans and D. L. Scharfetter, "Characterization of avalanche diode TRAPATT oscillators," *IEEE Trans. Electron Devices*, vol. ED-17, pp. 397–404, May 1970.

[4] M. Matsumara and H. Abe, "Computer simulation of anomalous mode oscillation in silicon avalanche diodes," *IEEE Trans. Microwave Theory Tech.* (Corresp.), vol. MTT-18, pp. 975–977, Nov. 1970.

[5] S. P. Yu and W. Tantraporn, "A computer simulation scheme for various solid-state devices," *IEEE Trans. Electron Devices*, vol. ED-22, pp. 515–522, Aug. 1975.

[6] J. O. Scanlan and T. J. Brazil, "Large-signal computer simulation of IMPATT diodes," *IEEE Trans. Electron Devices,* vol. ED-28, pp. 12–21, Jan. 1981.

[7] T. J. Brazil, Ph.D. Thesis, National Univ. of Ireland, May 1977.

[8] R. W. Hamming, *Numerical Methods for Scientists and Engineers.* New York: McGraw-Hill, 1973.

[9] J. Gonda and W. E. Schroeder, "IMPATT diode design for parametric stability," *IEEE Trans. Microwave Theory Tech.*, vol. MTT-25, pp. 343–352, May 1977.

[10] M. E. Hines, "Large-signal noise, frequency-conversion and parametric instabilities in IMPATT networks," *Proc. IEEE*, vol. 60, pp. 1534–1548, Dec. 1972.

[11] W. E. Schroeder, "Spurious parametric oscillations in IMPATT diode circuits," *Bell Syst. Tech. J.*, vol. 53, pp. 1187–1210, Sept. 1974.

[12] R. A. Giblin, E. F. Scherer, and R. L. Wierich, "Computer simulation of instability and noise in high-power avalanche diodes," *IEEE Trans. Electron Devices*, vol. ED-20, pp. 404–418, Apr. 1973.

[13] B. Culshaw, R. A. Giblin, and P. A. Blakey, "Avalanche diode oscillators: Part I, basic concepts," *Int. J. Electron.*, vol. 37, pp. 577–632, 1974.

[14] C. A. Brackett, "The elimination of tuning-induced burnout and bias-circuit oscillations in IMPATT oscillators," *Bell Syst. Tech. J.*, vol. 52, pp. 271–306, Mar. 1973.

[15] C. B. Swan, "IMPATT performance improvement with second harmonic tuning," *Proc. IEEE*, vol. 56, pp. 1616–1617, Sept. 1968.

[16] W. E. Schroeder and G. I. Haddad, "Effect of harmonic and subharmonic signals on avalanche-diode oscillator performance," *IEEE Trans. Microwave Theory Tech.*, vol. MTT-18, pp. 327–331, June 1970.

Sensitivity of the Total Power Radiometer with Periodic Absolute Calibration

MICHAEL S. HERSMAN, MEMBER, IEEE, AND GENE A. POE

Abstract—**The total power radiometer is an attractive choice for imaging applications due to its high sensitivity and simple configuration. However, available theoretical results are inadequate to allow an accurate radiometer performance prediction in the presence of receiver gain fluctuations and other receiver characteristics with nonuniform fluctuation power spectra. An improved analysis of the total power radiometer ΔT is presented in terms of the receiver output fluctuation power spectral density and a transfer function due to postdetection filtering and periodic calibration. Verification of this analysis is obtained by measuring the fluctuation power spectrum of a 94-GHz receiver and comparing the predicted ΔT with a direct measurement. Numerical results including application to an example radiometer system are presented. These results indicate that the total power radiometer should function well in short integration time, periodically calibrated radiometer systems.**

I. INTRODUCTION

MICROWAVE radiometry is rapidly becoming important in meteorological remote sensing, atmospheric sounding, and tactical reconnaissance [1]–[4]. These applications share the need for formation of a radiometric image, requiring many radiometric measurements in a limited time and placing extreme demands on radiometer performance. The total power radiometer offers the potential of providing the best sensitivity and the simplest realization of any common radiometer configuration, and is an attractive choice for imaging applications. However the total power radiometer has seen limited application for at least two reasons: 1) the performance is susceptible to degradation by receiver gain fluctuations, electronic $1/f$ noise, and other time varying receiver characteristics; and 2) available theoretical results are inadequate to permit accurate prediction of performance.

It has been common practice [5]–[8] to express the sensitivity of the total power radiometer in terms of the noise equivalent temperature difference

$$\Delta T = T_{sn}\sqrt{\frac{1}{B\tau}+\left(\frac{\Delta G}{G}\right)^2} \tag{1}$$

where T_{sn} is the equivalent radiometer input system noise temperature, and B and τ are, respectively, the predetection convolutional bandwidth, and the equivalent postdetection integration time. The quantity $\Delta G/G$ represents the normalized rms fluctuation of receiver power gain.

Although this equation provides a qualitative relation-

Manuscript received July 8, 1980; revised August 27, 1980.

The authors are with the Space and Communications Group, Hughes Aircraft Company, Los Angeles, CA 90009.

0018-9480/81/0100-0032$00.75 ©1981 IEEE

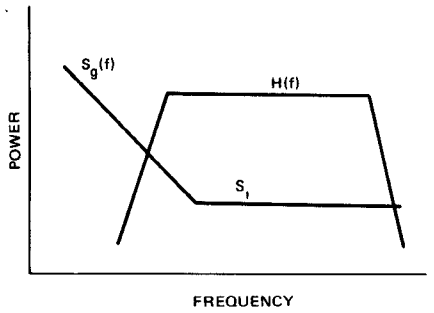

Fig. 1. Total power radiometer ΔT representation.

ship between $B\tau$, T_{sn}, $\Delta G/G$, and radiometer ΔT, it fails to account for the effects of noise in radiometer calibration measurements, and more importantly, it fails to provide a useful characterization of random gain fluctuation effects in terms of radiometer calibration parameters, such as calibration period and integration time.

This paper derives an expression for the sensitivity which removes these shortcomings. This is accomplished by analyzing the sensitivity in terms of the receiver output fluctuation power spectral density and a unitless transfer function $H(f)$ due to postdetection filtering and periodic calibration. This perspective is illustrated in Fig. 1. The receiver power spectrum is shown as the sum of a uniform component S_i, characteristic of ideal radiometer performance, and a $1/f^{\alpha}$ $(\alpha \neq 0)$ component $S_g(f)$, characteristic of a gain fluctuation spectrum. As may be expected, the calibration processor transfer function $H(f)$ is determined by radiometer scan and calibration parameters. The radiometer $(\Delta T)^2$ is proportional to the receiver fluctuation power in the calibration processor passband

$$(\Delta T)^2 = c^2 \int_0^{\infty} df S_r(f) H(f) \tag{2}$$

where c is a constant radiometer scale factor (K/volt), and $S_r(f) = S_g(f) + S_i(\mathrm{V}^2/\mathrm{Hz})$.

This paper is organized as follows. A preliminary discussion of the operation of a total power radiometer leads to a derivation of the calibration processor transfer function representation of the radiometer ΔT. Verification of this analysis is obtained by measuring the fluctuation power spectrum of a 94-GHz receiver and comparing the predicted ΔT with a direct measurement. The final section presents some numerical results and examines the performance of an example total power radiometer system.

II. Preliminaries

The total power radiometer consists of a receiver, which generates a signal proportional to input brightness temperature, and a calibration processor, which averages the receiver output and computes an estimate of the brightness temperature based on calibration measurements and known temperatures.

A common situation is shown in Fig. 2, in which a microwave total power receiver periodically interrupts scene measurements to view two blackbody calibration sources. The calibration temperatures T_1 and T_2 are generally chosen near the limits of the radiometer measurement range. For square law detector operation (postdetection voltage proportional to predetection power), the receiver generates a noisy output voltage $v(t)$ whose time average is proportional to $T_{sn} = T_s + T_r$, where T_s is the scene brightness temperature and T_r is the receiver equivalent noise temperature.

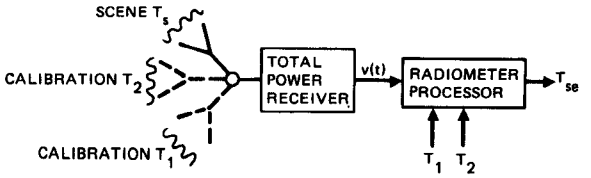

Fig. 2. Total power radiometer configuration.

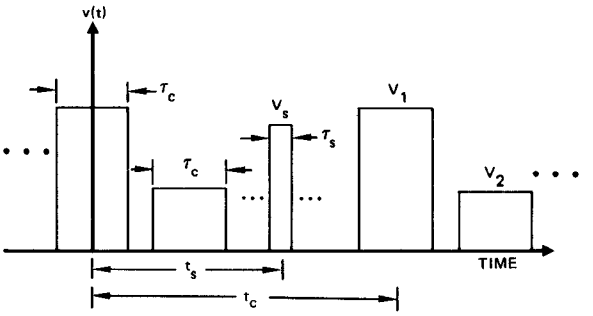

Fig. 3. Receiver output voltage characteristics.

Fig. 3 presents a description of a typical receiver output as a function of time, showing periodic measurements of the two receiver calibration sources and one of many scene measurements. The quantities τ_s, τ_c, t_c, and t_s, are, respectively, the scene integration time, the calibration integration time, the calibration period, and the calibration to scene measurement time. The radiometer processor in Fig. 2 averages the receiver output voltages over τ_c or τ_s and operates on the calibration receiver outputs and known calibration temperatures to compute an estimate of the brightness temperature associated with the scene voltage sample according to the linear relationship

$$T_{se}(t) = c(t)\left[\bar{V}_s(t) - V_{1e}(t)\right] + T_1 \tag{3}$$

where

$$c(t) = \frac{T_1 - T_2}{V_{1e}(t) - V_{2e}(t)} \tag{4}$$

and V_{1e}, V_{2e} are estimates of the radiometer calibration voltages $\bar{V}_1, \bar{V}_2$, averaged over τ_c, corresponding to T_1, T_2 at time t, and $\bar{V}_s$ is the output voltage associated with the scene temperature T_s, averaged over τ_s.

Equations (3) and (4) may be considered an estimate of the receiver state at the measurement time derived from estimates of the calibration voltages V_{1e} and V_{2e}. This estimation is required due to broad-band noise appearing in the measurement and calibration voltage samples, as well as slowly varying receiver characteristics, such as temperatures related gain drifts and other receiver noise sources with $1/f$ spectra. The $1/f$ noise contributes an

error that is related to the calibration to scene measurement time.

In the simplest case, only the single set of calibration values $(\bar{V}_1, \bar{V}_2)$ nearest the measurement time is used. However, significant performance improvements can be obtained using a more complex estimator of the calibration voltages.

In general, an estimate of $\bar{V}_1$ can be expressed as a convolution of noisy calibration values $\bar{V}_1(kt_c)$, indexed by $k=0, \pm 1, \pm 2, \cdots$, with time invariant weighting function $w(t-kt_c)$

$$V_{1e}(t)=\sum_k w(t-kt_c)\bar{V}_1(kt_c). \tag{5}$$

A similar estimation can be made of $\bar{V}_2$. Proper normalization requires

$$\sum_k w(t-kt_c)=1. \tag{6}$$

The weights and the number of calibration samples included in the estimator can be selected to conform to performance requirements, processing complexity, and other system considerations.

In general, the uncertainty in T_{se} arises from noise in V_s, V_{1e}, and V_{2e}. For scene temperatures T_s equal to the calibration temperature T_1, the variance in T_{se} to a first-order approximation may be expressed as

$$(\Delta T_{se})^2(t)=E\left\{\left[\bar{V}_s(t)-V_{1e}(t)\right]^2\right\}. \tag{7}$$

E is the ensemble expection operator. Note that the previous normalization condition (6) implies for processes possessing constant ensemble mean values

$$E\left\{\bar{V}_s(t)-V_{1e}(t)\right\}=0. \tag{8}$$

The contribution to ΔT_{se} from noise in c is second order.

For $T_s \neq T_1$ or T_2, it is straightforward to show

$$(\Delta T_{se})^2=c^2E\left\{\left[\beta\left(\bar{V}_s(t)-V_{1e}(t)\right)+(1-\beta)\left(\bar{V}_s(t)-V_{2e}(t)\right)\right]^2\right\} \tag{9}$$

where

$$\beta=\frac{T_s-T_2}{T_1-T_2}. \tag{10}$$

Both (7) and (9) assume that the fluctuation in $V_{1e}-V_{2e}$ is much less than the mean value. This permits a power series expansion of $c(f)$ in terms of the fluctuating part of $V_{1e}-V_{2e}$. Terms higher than first order may be neglected. In (9) c is evaluated with the mean values of V_{1e} and V_{2e}.

In the interest of clarity we restrict our analysis to the case in which T_s is equal to the higher calibration temperature T_1. This is a worst case for scene temperatures between or equal to the calibration temperatures, and simplifies the analysis.

The representation of the total power radiometer ΔT in terms of differences between the calibration and measurement values is an extension of the conventional representation (1), where only the fluctuation in the measurement value is considered.

III. Transfer Function/Power Spectrum Representation

A convenient expression for computing the maximum ΔT_{se} in the form of (2) may be obtained by expressing (7) in terms of the power spectral density of the receiver output voltage. Letting $v(t)$ denote the receiver output voltage at time t, then $\bar{V}_s-V_{1e}$ may be expressed as

$$\bar{V}_s(t)-V_{1e}(t)=\int_{-\infty}^{\infty}dt'\,v(t')\left[h_s(t-t')-\sum_k w(t-kt_c)h_c(kt_c-t')\right] \tag{11}$$

where

$$h_s(t)=\begin{cases}\dfrac{1}{\tau_s}, & |t|\leqslant\dfrac{\tau_s}{2}\\ 0, & |t|>\dfrac{\tau_s}{2}\end{cases}$$

$$h_c(t)=\begin{cases}\dfrac{1}{\tau_c}, & |t|\leqslant\dfrac{\tau_c}{2}\\ 0, & |t|>\dfrac{\tau_c}{2}\end{cases}$$

are impulse responses of the scene and calibration integration filters. Substituting (11) into (7) and interchanging the ensemble expectation and integration operations yields

$$(\Delta T_{se})^2=c^2\int_{-\infty}^{\infty}dt'\int_{-\infty}^{\infty}dt''E\{v(t')v(t'')\}\left[h_s(t-t')-\sum_k w(t-kt_c)h_c(kt_c-t')\right]\cdot\left[h_s(t-t'')-\sum_k w(t-kt_c)h_c(kt_c-t'')\right]. \tag{12}$$

Assuming that the receiver output $v(t)$ possesses a one-sided power spectral density $S_r(f)$ satisfying

$$\int_{f_l}^{f_h}df\,S_r(f)<\infty \tag{13}$$

then the autocorrelation function of $v(t)$ appearing in (12) may be represented formally as

$$E\{v(t')v(t'')\}=\lim_{\substack{f_l\to 0\\ f_h\to\infty}}\int_{f_l}^{f_h}df\,S_r(f)\cos\left[2\pi f(t'-t'')\right]. \tag{14}$$

The quantities f_l and f_h are low and high cutoff frequency limits which lead to finite values for the integrations in (13) and (14). Strictly speaking, the process of taking the limit operations in (14) can lead, for some spectral densities, to an ill-defined autocorrection function (e.g., $(S_r(f)=f^{-\alpha}$ with $\alpha>1$). However, for the spectral densities of interest herein the indeterminancy in (14) is unimportant

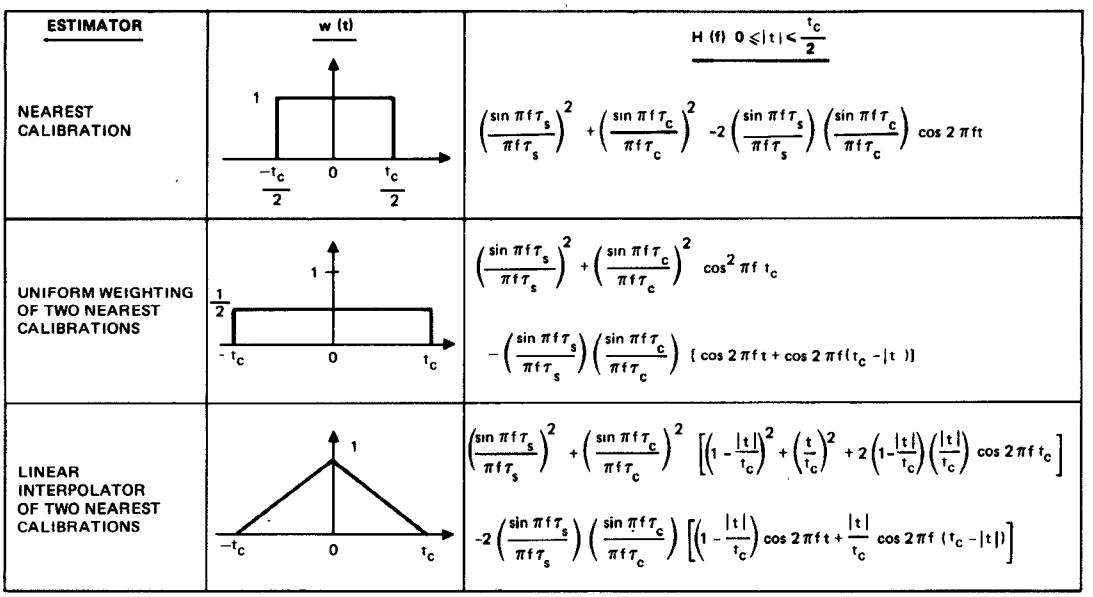

Fig. 4. Representative transfer functions.

in computing ΔT_{se} due to the bandpass filtering action of the functions appearing in brackets in (12). That is, the subtraction operation in (12) and the postdetection integration filters attenuation as $f_l \to 0$ and $f_h \to \infty$ so that the computation of ΔT_{se}^2 is independent of the limits. Thus, substituting (14) into (12), performing the indicated time integration, and taking the limits in (14) yields

$$\Delta T_{se}^2(\tau_s, \tau_c, T_c, t, w, S_r) = c^2 \int_0^\infty df S_r(f) H(f) \quad (15)$$

where

$$H(f) = \left| \frac{\sin \pi f \tau_s}{\pi f \tau_s} - \frac{\sin \pi f \tau_c}{\pi f \tau_c} \sum_k w(t - kt_c) e^{-j2\pi f(t-kt_c)} \right|^2. \quad (16)$$

The functional relationship between ΔT_{se} and the scene and calibration integration times τ_s and τ_c, the calibration interval t_c, the measurement time t_s, the calibration estimator weighting function $w(t)$, and the receiver power spectrum S_r, is explicitly shown. The vertical bars denote complex absolute value and $j = \sqrt{-1}$.

Equation (15) provides a convenient means of computing the maximum ΔT_{se} of a total power radiometer given the receiver power spectral density and the scan and calibration parameters. Equation (15) may be expressed in more familiar form by considering $S_r(f)$ as the sum of uniform S_i and nonuniform $S_g(f)$ spectral densities. For the total power receiver S_i may be represented by [6]

$$S_i(f) = \frac{2T_{sn}^2}{c^2 B}, \qquad 0 \leq f \ll B \quad (17)$$

where c is a scale factor (4), B is the receiver bandwidth (1), and T_{sn} is the input system noise temperature when $T_s = T_1$.

Substituting (17) into (15) for the uniform component of the receiver power spectrum yields a useful expression for the normalized total power radiometer ΔT_{se}

$$\left(\frac{\Delta T_{se}}{T_{sn}}\right)^2 = \frac{1}{B\tau_s} + \frac{1}{B\tau_c} \sum_k w^2(t - kt_c) + \left(\frac{\Delta G}{G}\right)^2 \quad (18)$$

where

$$\left(\frac{\Delta G}{G}\right)^2 = \left(\frac{c}{T_{sn}}\right)^2 \int_0^\infty df S_g(f) H(f). \quad (19)$$

The first term in (18) corresponds to the fluctuation in the scene measurements due to S_i. The second term corresponds to the fluctuation in the calibration estimation due to S_i, and the final term describes the contribution to ΔT_{se} from S_g, and includes both the scene and calibration contributions.

Equations (18), (19), and (16) remove the deficiencies noted earlier in the conventional expression for the total power radiometer $\Delta T(1)$. The effect of uniform noise on the calibration is represented by the second term of (18), and an explicit expression is given to compute the effect of receiver gain fluctuations (19) and (16). In the following sections, the subscript *se* on ΔT is understood. An examination of the characteristics of $H(f)$ is presented in the next section.

IV. Example Transfer Functions

It is informative to examine $H(f)$ for three simple estimator weighting functions. Fig. 4 presents $w(t)$ and a closed form expression of $H(f)$ for the nearest calibration, uniform weighting of two nearest calibrations, and linear interpolation of two nearest calibrations. Computer generated plots of $H(f)$ for the three calibration estimators of Fig. 4 are presented in Figs. 5, 6, and 7.

Fig. 5 shows $H(f)$ for the nearest calibration estimator, both for a single measurement time $t_s = t_c/4$, curve *A*, and averaged over the entire scan, $|t_s| < t_c/2$, curve *B*. There are three major regions of interest. In the low frequency

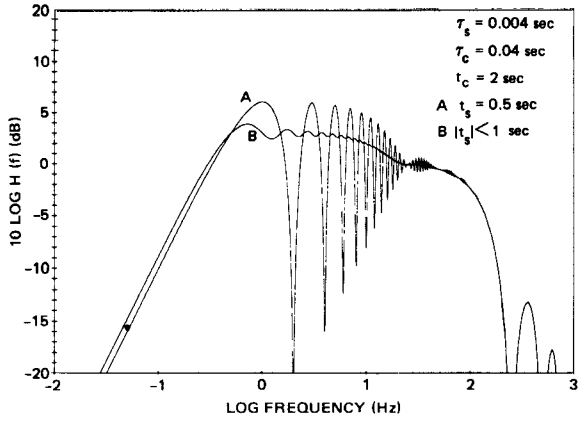

Fig. 5. Nearest calibration transfer function.

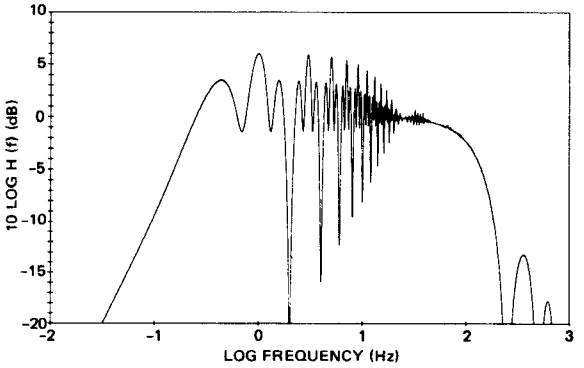

Fig. 6. Uniform weighting transfer function.

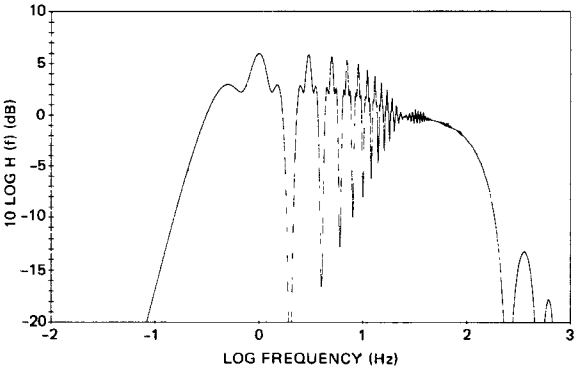

Fig. 7. Linear interpolator transfer function.

region, $f<1/2t_c$, $H(f)$ approaches zero as f^{-2}. In the calibration integrator passband, $1/2t_c<f<1/2\tau_c$, $H(f)$ has a peak value of +6 dB and an average value of +3 dB. This is a result of the combined uncertainty in the calibration and scene measurements, including effects of the phasing due to the calibration to scene measurement time t_s. In the high frequency region, $f>1/2\tau_c$, $H(f)$ has the $\sin x/x$ behavior characteristic of the scene integrator.

For more complex calibration estimators the choice of $w(t)$ influences the form of $H(f)$. Fig. 6 shows $H(f)$ for the uniform weighting of the nearest two calibrations and Fig. 7 shows $H(f)$ for the linear interpolator using the same data presented in Fig. 5 for curve A. It is seen that the low frequency performance of the linear interpolator, which approaches zero as f^{-4}, is superior to the uniform weighting estimator with its f^{-2} behavior. This results in improved rejection of the nonuniform component of the receiver power spectrum. However, uniform weighting minimizes $w^2(t-kt_c)$ (18), which results in superior radiometer performance in the presence of a uniform receiver power spectrum. Given a receiver power spectrum, and the desired radiometer scan and calibration parameters, a $w(t)$ can be selected using standard mathematical techniques to minimize the radiometer ΔT.

V. Experimental Verification

The results of the previous analysis were tested by comparing the radiometer ΔT predicted by (15) with a direct time sampled estimate suggested by (7)

$$\Delta T_{se}^2 \cong \frac{c^2}{N} \sum_{i=1}^{N} \left[\bar{V}_s(t_i) - V_{1e}(t_i) \right]^2. \tag{20}$$

This test involved assembling a total power radiometer, measuring its receiver output fluctuation power spectrum, predicting the radiometer ΔT using (15), and comparing the predicted ΔT to a direct measurement over a range of calibration periods.

A. Receiver Description

The radiometer receiver block diagram is shown in Fig. 8. It consists of a 94-GHz balanced mixer/preamplifier driven by a Gunn diode local oscillator, an IF amplifier, and a tunnel diode detector/video amplifier. The mixer/preamplifier, which has been described in the literature, [9] exhibits an average 5.5-dB double sideband noise figure over an IF bandwidth of 1.5 GHz using a discrete component IF preamplifier and planar diodes in a biased configuration. The receiver temperature coefficient of gain was measured and found to be -7×10^{-3} or -0.03 dB/°C. The power spectrum and ΔT measurements are largely independent of temperature drift effects due to the care taken in providing a temperature controlled radiometer enclosure. This is done to improve measurement repeatability. The receiver is mounted in a 1/4-in aluminum box, which is inside an insulating foam enclosure along with a large amount of metal for increased thermal mass. The receiver temperature is controlled with a first order controller which integrates any steady-state temperature error to zero. The peak to peak temperature sensor fluctuation was about 5×10^{-4}°C, but the large size and temperature gradients present in the radiometer enclosure resulted in an infrequent worst case average receiver temperature drift of 0.05°C/h, as evidenced by the receiver output drift. These temperature drifts have a small influence on the lowest frequency samples of the power spectrum. Quantitative effects of these drifts are discussed below in relation to the direct ΔT measurements. Interference effects from local transmitters were also encountered, so the measurements were done in a screen room.

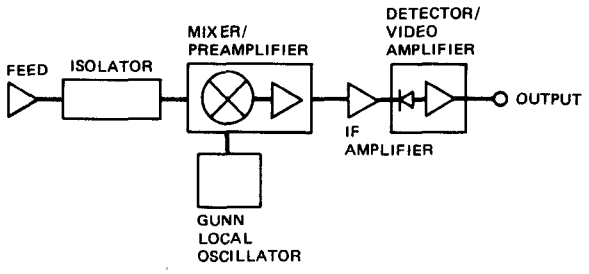

Fig. 8. Total power receiver block diagram.

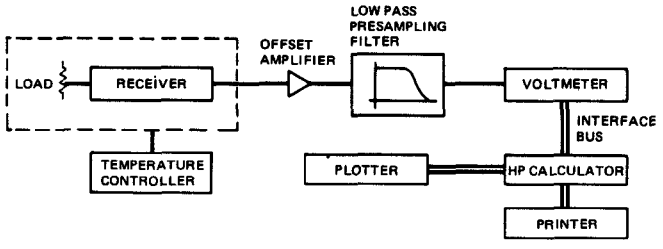

Fig. 9. Measurement system block diagram.

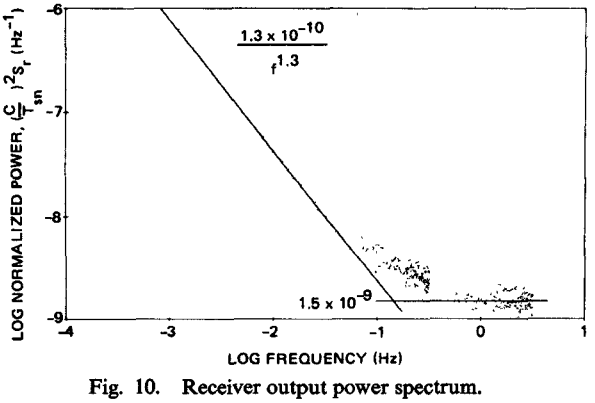

Fig. 10. Receiver output power spectrum.

B. Receiver Power Spectral Density Measurement

The arrangement for measuring the receiver output power spectrum is shown in Fig. 9. The receiver output is applied to a dc coupled amplifier with adjustable offset, which is used to amplify the small receiver output fluctuations and remove the large dc component of the receiver output. A low-pass presampling filter with a four pole Butterworth response is used to eliminate signal components with frequencies above one-half the sampling frequency of the data acquisition system.

The data acquisition and analysis system consists of a Hewlett-Packard 9825 calculator controlling a voltmeter, plotter, and printer. The power spectrum is calculated as the square of the discrete Fourier transform of the radiometer output waveform. To reduce the variance of the spectral density estimate, 20 independent measurements of the power spectrum are averaged.

The results of the measurement are shown in Fig. 10, with units of (normalized fluctuation)^2 Hz^{-1}. This is a plot of two overlapping sets of data, each containing 512 points. One set covers the frequency range from 6.25×10^{-4} Hz to 0.32 Hz with a resolution of 6.25×10^{-4} Hz. The second set covers frequencies from 6.25×10^{-3} Hz to 3.2 Hz with a resolution of 6.25×10^{-3} Hz.

As expected, the measured receiver power spectrum is the sum of two major components. At low frequencies the $1/f$ character of the gain fluctuation noise is large, while at frequencies above 1 Hz a uniform spectrum resulting from ideal radiometer characteristics is apparent. In addition, there is a small amount of noise contributed by the video amplifier electronics which is measured separately and accounts for the difference between the measured power spectrum and the sum of the uniform and $1/f$ components in the vicinity of 0.2 Hz. The solid lines are visual estimates of the major power spectrum components.

A check on the accuracy of the spectral measurement can be made by comparing the measured value of the uniform spectrum to the theoretical normalized value of $2/B$ (17). For the receiver, $B=1.53$ GHz, resulting in a theoretical normalized uniform spectrum of amplitude 1.3 10^{-9}/Hz. This is within 15 percent of the measured value of 1.5×10^{-9}/Hz. The video amplifier noise is responsible for less than 5-percent contribution at 3 Hz.

Measurements with a second mixer containing wisker contacted Schottky diodes and a modular IF preamplifier were very similar, indicating that the magnitude and shape of the receiver output power spectrum is not affected by differences between these two mixer/preamplifier/local oscillator sets.

C. Direct ΔT Measurements

It is worthwhile to test the validity of the transfer function/power spectrum model of radiometer ΔT with a direct measurement (20) for a range of calibration to measurements times t_s.

The model predicts that an increase in t_s (and t_c) results in an increase in radiometer ΔT due to reduced rejection of S_g, the $1/f^{\alpha}$ component of the power spectrum. To emphasize this effect it is desirable to eliminate as much of the uniform receiver noise as possible by using a long integration time postdetection filter. For this test a 3-s integrate and dump was used, resulting in a transfer function residing largely in the $1/f$ region of the receiver spectrum. For this measurement, (20) becomes

$$\Delta T^2 \cong \frac{c^2}{N}\sum_{i=1}^{N}\left[\bar{V}(t_{i+1})-\bar{V}(t_i)\right]^2 \qquad (21)$$

where $\bar{V}$ represents a series of $N+1$ samples of the radiometer output integrator, spaced at t_s. The nearest calibration analysis applies, with $\tau_c=\tau_s=3$ s, t_s variable. Note that for the nearest calibration, $t_c \geq 2t_s$. The results of this measurement over $t_s=3.33$ to 1000 s are shown in Fig. 11.

The solid line represents the predicted value of radiometer ΔT using the power spectrum of Fig. 10 and the nearest calibration transfer function in Fig. 4. The data points represent the measured values of ΔT for $N=300$. Although there is a slight bias apparent in the measured values, the overall agreement is good. The bias is consis-

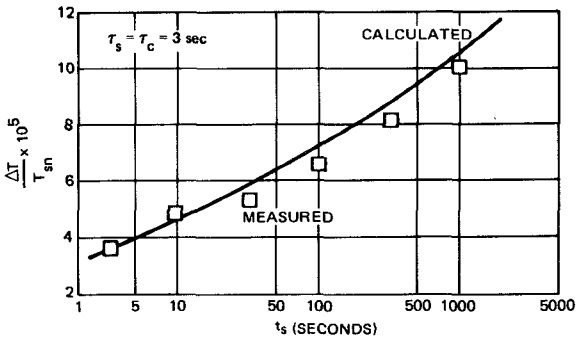

Fig. 11. Calculated and measured radiometer ΔT.

tent with the 15-percent difference between the calculated and measured values of the uniform component of the radiometer output spectrum mentioned previously.

During the ΔT measurements the mean value of the voltage differences (21) was also computed to enable the contribution of linear radiometer drifts to the measured ΔT to be estimated. A ΔT measurement of a linear drift would yield an average difference value equal to the rms value, while the measurement of a random process would yield an average near zero.

During these ΔT measurements the average value was in all cases less than 10 percent of the rms value and in most cases was less than 1 percent. This indicates that the linear drifts present in the receiver had a negligible effect on the ΔT measurement.

This measurement demonstrates the validity of the receiver power spectrum/processor transfer function representation of the radiometer ΔT, which provides an accurate means of predicting radiometer performance for a wide range of scan parameters.

VI. System Application

The performance of an ideal total power radiometer ($S_g = 0$) can easily be calculated in closed form using (18), but accurate determination of gain fluctuation effects must be obtained by integrating the product of the measured $1/f^{\alpha}$ component of the receiver output power spectrum and the processor transfer function. Presentation of numerical $\Delta G/G$ results for a range of scan parameters using the receiver output power spectrum previously measured provides an estimate of the gain fluctuation effects to be expected in various systems and insight into the tradeoffs involved.

From (18) and (19) it is seen that $\Delta G/G$ is a function of the radiometer parameters $\tau_s, \tau_c, t_c, w, S_g$. The assumption is made that S_g follows the power law observed at low frequencies over the frequency range of interest. Results will be presented for w corresponding to the nearest calibration and linear interpolator estimators, with $t_s = 0.5\ t_c$ (scan midpoint) and $S_g = 1.3 \times 10^{-10}/f^{1.3}$ Hz^{-1} (normalized), the value estimated from the previous measurements.

In systems where time allows, increasing τ_c relative to τ_s decreases the noise in the calibration measurement, reducing the ΔT. In the following computations, $\tau_c = 10\tau_s$, which

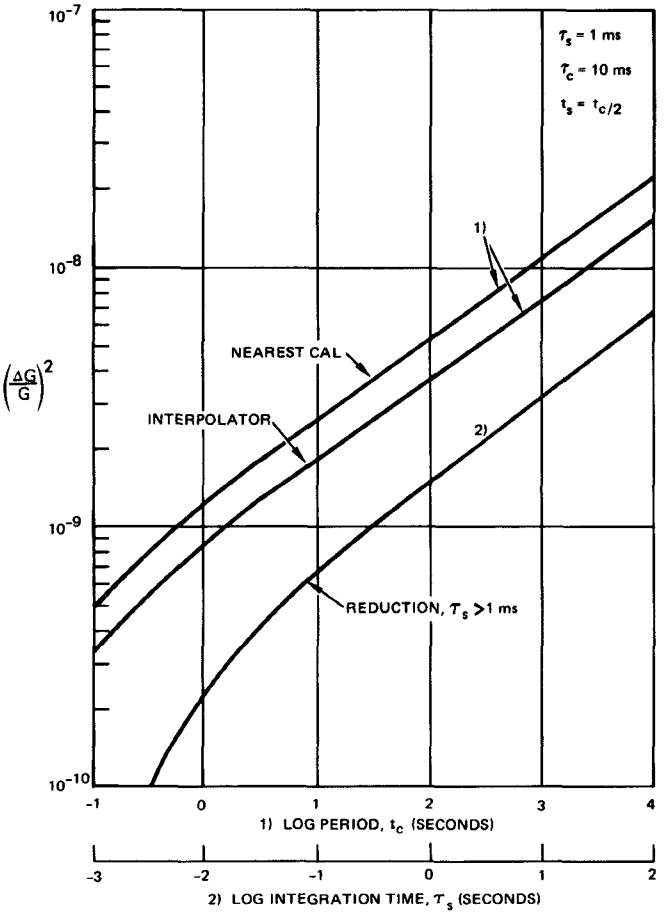

Fig. 12. Radiometer $(\Delta G/G)^2$.

results in a contribution to ΔT from uniform spectrum calibration noise of less than 5 percent.

Fig. 12 shows the caluclated value $(\Delta G/G)^2$ for a radiometer with $\tau_s = 1$ ms, $\tau_c = 10\tau_s$, $t_s = t_c/2$, and $0.1 < t_c < 10\ 000$ s. Values are shown for both the nearest sample and linear interpolator calibration procedures.

Increasing τ_s (and $\tau_c = 10\tau_s$) lowers the high frequency limit of the radiometer transfer function and reduces the radiometer $(\Delta G/G)^2$. This reduction is also plotted in Fig. 12 as a function of integration time τ_s, and must be subtracted from the $(\Delta G/G)^2$ for $\tau_s > 1$ ms. For example, the receiver tested previously, used in a nearest calibration radiometer with $t_c = 4$ s and $\tau_s = 1$ ms would exhibit a $(\Delta G/G)^2$ of 2×10^{-9}. Increasing τ_s to 4 ms results in a reduction in $(\Delta G/G)^2$ of 1×10^{-10} to 1.9×10^{-9}. For systems with $\tau_c = 10\tau_s$ the upper limit of $\tau_s \approx 1/30T_c$, which allows time for two calibration measurements (T_1 and T_2) and ten scene measurements.

The dependence of gain fluctuation effects on calibration interval t_c leads to a maximum useable t_c under the condition that gain fluctuation effects not dominate radiometer ΔT

$$\left(\frac{\Delta G}{G}\right)^2 \leqslant \frac{1}{B\tau_s}. \tag{22}$$

The equality is plotted in Fig. 13 for the nearest calibration and linear interpolator estimators as a function of τ_s

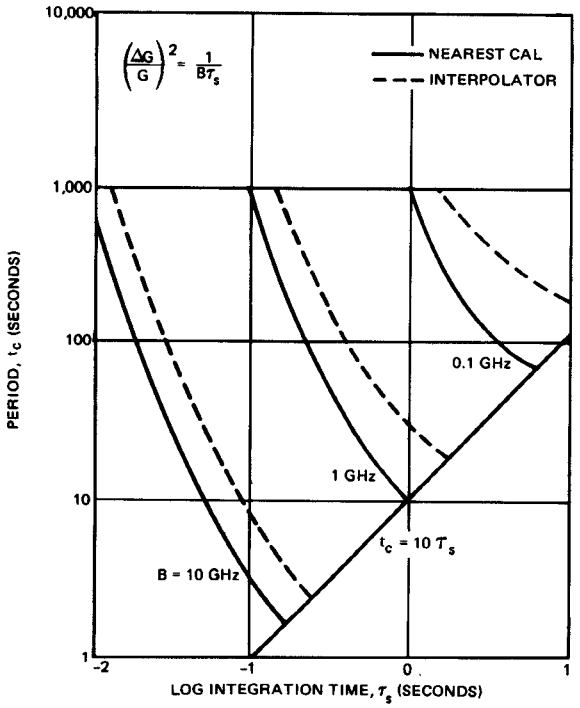

Fig. 13. CAL period/integration time trade.

and t_c with B as a parameter. Note that, for short integration times (<10 ms) and reasonable IF bandwidths (<10 GHz), calibration intervals in excess of 1000 s (≈15 min) can be used with only moderate degradation of the radiometer ΔT. This is a surprisingly long calibration interval and indicates that the effect of $\Delta G/G$ should be small in radiometers which are calibrated every few seconds.

Temperature related gain drifts, which are influenced by the radiometer design and operating environment have not been included in this analysis. However, temperature effects can be large, especially for long calibration intervals, and are easily incorporated into the radiometer ΔT model.

Temperature effects should be uncorrelated with the previously considered contributions to ΔT and thus add independently to the variance (18). If the receiver power spectrum $S_r(f)$ can be measured with the receiver in its expected operating environment, temperature effects will contribute to $S_r(f)$ and be included in the analysis. If this is not possible, the magnitude of the temperature effects can be estimated in a manner similar to (19) given the power spectrum of the expected receiver operating temperature or by using an expression similar to (20) given a temperature time record. In both cases the receiver output fluctuation is related to the temperature changes using the receiver temperature coefficient of gain, and the temperature related variance adds as a fourth term to (18).

It is interesting to examine the performance of a total power radiometer, the Special Sensor Microwave/Imager (SSM/I), using the analytical and experimental results presented in the previous sections. The SSM/I is currently being built by Hughes Aircraft Company to fly on the RCA Block 5-D spacecraft as part of the U.S. Air Force Defense Meteorological Satellite Program.

TABLE I
SS/I 85-GHz Channel Parameters

Parameter	Value
τ_s	4.0 ms
τ_c	20 ms ($5\tau_s$)
t_s	2.0 sec (max)
B	1.50 GHz
T_{sn}	2000K
$S_g(f)$	$1.3 \times 10^{-10}/f^{1.3}$ Hz^{-1}
$\left(\frac{\Delta G}{G}\right)^2$	1.86×10^{-9}
$\Delta T\,(S_i)$	0.899K (with $S_g = 0$)
$\Delta T\,(S_r)$	0.903K

The SSM/I is a seven channel four frequency conically scanning radiometer with two channels (dual polarization) at 19 GHz, 37 GHz, and 85 GHz and a single channel at 22 GHz. It completes a scan and calibration sequence every 2 s and uses the nearest previous calibration value, resulting in a worst case calibration to scene measurement time of nearly 2 s. The performance of this calibration procedure is equivalent to that of a 4-s period, nearest calibration procedure.

The information required to calculate the radiometer ΔT from (18) for the SSM/I 85-GHz channel is given in Table I. The contribution of calibration and gain fluctuation effects to the total radiometer ΔT can be determined by examining the magnitude of the three terms on the right-hand of (18).

The first term, which represents the fluctuation in the scene measurements due to the uniform component of the receiver power spectrum S_i is equal to 1.67×10^{-7}. The second term, representing the fluctuation in the calibration measurements due to S_i is 3.33×10^{-8}. The summation (18) is equal to unity when only one calibration value is used.

The third term in (18), which represents the fluctuation due to the nonuniform component of the receiver power spectrum $S_g(f)$ is 1.86×10^{-9}. This value was calculated using (19) and (16).

The SSM/I ΔT is presented in Table I with and without the influence of $S_g(f)$. Comparison shows that the SSM/I suffers very little performance degradation from gain fluctuations, which allows the SSM/I to use a total power radiometer, resulting in a simple, high performance system.

VII. Conclusion

An improved analysis of the total power radiometer sensitivity has been presented in terms of the receiver output fluctuation power spectral density and a calibration processor transfer function. This analysis allows, for the first time, accurate prediction of radiometer performance for receivers with nonuniform output fluctuation power spectra. Good agreement between the analysis and experimental measurements has been obtained. Calcu-

lation of gain fluctuation effects using an example measurement of a receiver power spectrum indicate that the total power radiometer should function well in short integration time, periodically calibrated radiometer systems.

ACKNOWLEDGMENT

The authors wish to than E. Grant for valuable discussions, M. Calderon for assistance with the experimental measurements, and F. Goodwin and A. Edgerton for encouragement and support.

REFERENCES

[1] P. Gloersen and F. T. Barath, "A Scanning multi-channel microwave radiometer for Nimbus-G and SEASAT-A," *IEEE J. Oceanic Eng.*, vol. OE-2, pp. 172–178, Apr. 1977.
[2] Special Sensor Microwave Imager, SSM/I, Air Force Contract F04701-79-C-0061, awarded to Hughes Aircraft Co., 1979.
[3] H. N. Kritikos and J. Shiue, "Microwave sensing from orbit," *Spectrum*, vol. 16, no. 8, pp. 34–41, Aug. 1979.
[4] J. H. Rainwater, "Radiometers: Electronic eyes that 'see' noise," *Microwaves*, vol. 17, no. 9, pp. 58–62, Sept. 1978.
[5] M. E. Tiuri, "Radio astronomy receivers," *IEEE Trans. Antennas Propagat.*, vol. AP-12, pp. 939–947, Dec. 1964.
[6] J. D. Kraus, *Radio Astronomy*. New York: McGraw-Hill, 1966, p. 242.
[7] J. M. Schuchardt, "Detected noise levels guide radiometer design," *Microwaves*, vol. 17, no. 9, pp. 64–74, Sept. 1978.
[8] J. C. Bremer, "Improvement of scanning radiometer performance by digital reference averaging," *IEEE Trans. Instrum. Meas.*, vol. IM-28, pp. 46–54, Mar. 1979.
[9] A. G. Cardiasmenos, "Planar Devices Make Production Practical," *Microwave Syst. News*, vol. 9, no. 5, pp. 46–56, May 1979.

A Variational Expression for the Scattering Matrix of a Double-Step Discontinuity in a Coaxial Line and Its Application to a TEM Cell

IPPALAPALLI SREENIVASIAH, MEMBER, IEEE, AND DAVID C. CHANG, SENIOR MEMBER, IEEE

***Abstract*—A variational expression for the scattering matrix of a double-step discontinuity in a two-mode coaxial transmission line is obtained and generalized to the case of a multimode coaxial transmission line. The result is used to analyze the transmission characteristics of a two-mode coaxial TEM cell.**

I. INTRODUCTION

IT IS WELL KNOWN in transmission line design that the effect of a step discontinuity, resulting from a change in inner and/or outer radius of a coaxial line system, may be represented by an equivalent shunt susceptance. Expressions for such an equivalent shunt susceptance have been reported in literature [1]–[4] under the assumption that only the dominant TEM mode can propagate on either side of the discontinuity. Since a propagating mode can carry power, such a representation will no longer be valid whenever a higher order mode starts to propagate on either side of the discontinuity. A more general form of representation is then needed.

A typical example which demonstrates the need to develop a more general representation is that of a TEM cell used for low frequency electromagnetic radiation and susceptibility measurements of electronic equipment. In order to locally simulate, at low frequencies, a plane wave environment in a test area as in the case of an anechoic chamber used at higher frequencies, a coaxial structure capable of supporting a fundamental mode without cutoff, i.e., TEM mode, may be devised. Such a device is truncated at two ends and connected to standard coaxial lines where the transmission and the reflection of electromagnetic signals can be conveniently measured [5]. In the case when the test chamber is created by two concentric cylinders (rather than a rectangular hollow cylinder with a center septum as typically the case), the truncation at the two ends results in a double step discontinuity if the characteristic impedance on either side of the discontinuity is to remain the same. Now since the TEM cell (test

Manuscript received May 12, 1980; revised August 27, 1980. This work was supported by the National Bureau of Standards, Boulder, CO, under Contract DOC CST-8447.

The authors are with the Electromagnetics Laboratory, Department of Electrical Engineering, University of Colorado, Boulder, CO 80309.

0018-9480/81/0100-0040$00.75 ©1981 IEEE